Effect of ausforming temperature on creep strength of G91 investigated by means of small punch creep tests

Vivas, J.; Capdevila, C.; Altstadt, E.; Houska, M.; Serrano, M.; De-Castro, D.; San-Martin, D.;

Originally published:

June 2018

Materials Science and Engineering A 728(2018), 259-265

DOI: https://doi.org/10.1016/j.msea.2018.05.023

Perma-Link to Publication Repository of HZDR:

https://www.hzdr.de/publications/Publ-27384

Effect of Ausforming Temperature on Creep strength of G91 investigated by means of Small Punch Creep Tests

J. Vivas[1], C. Capdevila[1], E. Altstadt[2], M. Houska[2], M. Serrano[3], D. De-Castro[1], D. San-Martín[1]

[1]Materalia Research Group, Physical Metallurgy Department, Centro Nacional de Investigaciones Metalúrgicas (CENIM-CSIC), Avda. Gregorio del Amo 8, 28040 Madrid, Spain.

[2] Helmholtz-Zentrum Dresden - Rossendorf (HZDR), Dresden, Germany

[3]División de Materiales Estructurales, Centro Investigaciones Medioambientales y tecnológicas (CIEMAT), Avda. Complutense 22, 28040 Madrid, Spain.

Abstract

The stability of the martensitic microstructure in ferritic/martensitic G91 steel at operating temperatures up to 700 ºC might be improved by means of ausforming thermomechanical treatments. The goal sought is to promote the formation of a high number density of MX nanoprecipitates in the martensitic microstructure obtained after a subsequent tempering. This work is focused on the effect of the ausforming temperature. The results show that the lower the ausforming temperature is the higher is the dislocation density obtained in ausformed fresh martensite and the larger the number density of MX carbonitrides after tempering are. Creep strength, evaluated by Small Punch Creep Tests has allowed us to conclude that the best creep behavior was obtained for the steel ausformed at lower the temperature due to the higher pinning force for dislocation motion triggered by the distribution of MX. The creep results obtained on the ausformed samples were compared with those after the conventional heat treatment, showing that the high density of MX carbonitrides after an ausforming thermomechanical treatment is a promising processing to raise the operation temperature of this steel.

Keywords: Creep resistant steels; carbonitrides precipitation; martensite; tempering; small punch creep tests; ausforming.

1. Introduction

High Cr ferritic-martensitic (FM) steels are used as structural materials for fossil and nuclear power plants. Due to the new environmental regulations and commercial demands, there is a strong interest to improve creep strength of these steels to implement the operating temperatures above 650 °C [1-7]. The creep strength for these materials is provided by solid-solution and dispersion strengthening. Commonly 9% Cr ferritic-martensitic steels possess a hierarchal microstructure, i.e., prior austenite grains, martensitic packets, blocks and laths [8]. The microstructural degradation during creep is attributed to the coarsening of the subgrain/lath martensitic structure [9]. The dispersion of precipitates plays an important role in the stability of the martensitic microstructure at high temperatures. Precipitates pin boundary migration and dislocation motion slowing down the degradation of the martensitic microstructure at high temperatures, and hence reducing creep rates [10, 11].
It has been widely reported that there are two different kinds of particles that precipitate in 9Cr ferritic-martensitic steels during tempering: The $M_{23}C_6$ carbides, rich in chromium, which are located mainly at prior austenite grain, block and lath boundaries. The other kind of precipitate is the MX carbonitrides, rich in vanadium and niobium. The latter ones, in contrast to $M_{23}C_6$ carbides, are homogeneously distributed within laths. The effect of these two types of precipitates on the creep performance at high temperatures is the opposite. The $M_{23}C_6$ carbides are undesirable precipitates since their fast coarsening induces crack formation at the particle-matrix interface. On the contrary, the homogeneous distribution of nano-sized MX carbonitrides will delay the subgrain/lath coarsening as it has been studied extensively for creep conditions [12-14]. Therefore, many works have aimed to increase the number density of the more stable MX carbonitrides. Thermomechanical treatments have been reported as a promising processing route to obtain a high number density of MX carbonitrides [15-23]. Thermomechanical treatments involve different steps that need to be optimized to produce the most favorable precipitate microstructure for elevated temperature strength. This paper is focused on studying the effect of the ausforming temperature on MX carbonitrides distribution and size in the subsequent tempered martensite microstructure. The creep performance of the martensitic microstructure generated is evaluated by means of the small punch technique. The Small Punch Tests (SPT) have been used to estimate the ductile-to-

brittle transition temperature, mechanical strength and fracture toughness in situations where only small amounts of material are available [24-30]. Recently, the Small Punch Creep Test (SPCT) has been used to determine the creep properties in welding joints and new alloys [31-37]. The results suggest that the SPCT is a promising technique to monitor the creep behavior.

2. Materials and experimental procedure

The chemical composition of the commercial G91 ferritic-martensitic steel used in this work is shown in table 1.The thermomechanical treatments were carried out on cylindrical samples ∅5 x 10 mm using a 805 DIL Bahr plastodilatometer. The samples were heated at 5 ºC /s and cooled at 50 ºC /s. The deformation applied in the thermomechanical treatment was 20% at a deformation rate of 0.1 s^{-1} and the deformation temperature was 900 ºC and 600 ºC respectively. Figure 1 illustrates a scheme of the thermomechanical treatments.

Samples were prepared by conventional metallographic techniques, polishing down to 1 μm with diamond paste for microstructural examination by light optical microscopy (LOM) and scanning electron microscopy (SEM). The microstructure was revealed by Vilella's reagent, containing 5 ml hydrochloric acid, 1 g of picric acid and 100 ml of ethyl alcohol. This chemical etching discloses carbides and ferrite. Transmission electron microcopy (JEOL JEM 2100 and JEOL JEM 3000F), was used to observe the precipitates present in the microstructure. Disks of 3 mm in diameter and 120 μm in thickness were cut to prepare TEM samples. Disk thickness was reduced by mechanical grinding and final electropolishing (Tenupol 5) with a 95/5 acetic/perchloric acid solution at 298 ºC and 40 V.

Quantitative X-Ray diffraction analysis was performed on samples mounted in epoxy resin, ground, polished down to 1 μm diamond paste and a final polishing with 50 nm colloidal silica suspension. X-Ray diffraction measurements were performed by means of a Bruker AXS D8 diffractometer equipped with a Co-K_α X-ray tube with a Goebel mirror optics and a LynxEye Linear Position Sensitive Detector for ultra-fast XRD measurements. For the Rietveld refinement of the diffractograms, the version 4.2 program TOPAS has been used and the crystallographic information of the phase was obtained from Pearson´s Crystal Structure Database for Inorganic Compounds. The contribution of the microstrain is evaluated from the width of the diffraction peaks by means of the Warren-Averbach method [38, 39]. Once the microstrain is determined, the dislocation density is evaluated taking the most accepted formula in the literature that relates both [40, 41]. Due to the limited amount of material available after thermomechanical treatments carried out in the plastodilatometer, the creep properties were investigated by means of SPCT performed at 700 ºC with the parameters

shown in Table 2. SPCT samples were cut transversally, from cylindrical specimens, with a thickness of 600 μm and a diameter of 8 mm. Then, the discs were ground on both sides down to a final thickness of 500 μm. In the set-up of the SPCT, the lower and upper die are connected via a thread to ensure the clamping of the sample. The load is applied by a ceramic punch ball which is in contact with the sample. A plunger rod is used to transmit the dead weight load to the punch ball. All these components are made of Al_2O_3 ceramics. The clamping device is surrounded by an electrical heater and a thermal insulation. The upper plate carrying the additional dead weight is guided by to pillars with ball-bearings. The temperature is measured in the lower die directly under the sample. The displacement is measured by a capacitive sensor between the upper plate and the thermal insulation with an accuracy of ±1 μm. A load cell is placed between upper plate and plunger rod.
The upper plate with the dead weight can be locked by an electric spindle. This enables the start of the loading of the sample after heating-up and reaching the thermal equilibrium of the set-up. The experimental set-up is completely covered by an air-tight shell which is evacuated and flooded with Ar prior to the test. The whole set-up is shown in Figure 2. All SPC tests were performed in an Ar atmosphere with a nominally constant force resulting from the dead weight. The loading of the sample started after Ar flooding and heating-up.

3. Results and discussion

3.1. Microstructures of the steels prior to creep tests.

The steels involved in this investigation were processed as can be seen in Fig. 1. The materials were initially austenitized at 1225ºC to assure that most of the alloying elements are in solid solution in the austenite. As delta ferrite might be formed at such elevated temperatures as others authors have reported. This phase deteriorates the creep properties by provoking inhomogeneous deformation during creep [42, 43]. Appropriate precautions have been taken to avoid the formation of delta ferrite. In this sense, the austenitization temperature was selected as the maximum temperature without the formation of delta ferrite according to thermodynamic calculations made by Thermocalc®. The next stage in the thermomechanical treatment is the ausforming. In this stage, austenite is deformed in order to introduce dislocations which will act as nucleation sites for precipitates in the subsequent tempering. Miyamoto et al [44] reported a detailed description of the effect of ausforming on low-carbon lath martensite. The authors described that martensite variants with habit planes, i.e. $(575)_\gamma$, that are nearly parallel to the close-packed primary and secondary slip planes in austenite, i.e.

$(111)_\gamma$ and $(-111)_\gamma$, nucleate and grow preferentially [45]. Therefore, strain accumulated during ausforming results in increasing number of dislocation in $(111)_\gamma$ and $(-111)_\gamma$ slip planes that might be transferred to martensite $(011)_M$ planes. In this sense, ausforming might increase the dislocation density in martensite.

On the other hand, Takahashi et al. reported recently the formation of Nb-cottrell atmospheres in low-carbon Nb-microalloyed steels since the segregation energy of Nb to edge dislocation core was almost the same as grain boundary segregation energy, and the large attractive interaction between Nb and dislocation was due to its large atomic size. Such interaction Nb-dislocation retards the recovery of dislocation at high temperatures[46]. In the steel investigated we could be expected that Nb behaves in a similar way retarding recovery after ausforming and promoting fine and homogeneous MX carbonitrides during tempering

As it has been mentioned, two different ausforming temperatures were studied, 600 ºC and 900 ºC, at 20 % of deformation. Dislocation densities were determined by XRD in fresh martensite after each ausforming processing. Values of $2.8\pm0.1\cdot 10^{15}$ m^{-2} and $1.9\pm0.1\cdot 10^{15}$ m^{-2} were obtained for the ausforming at 600 ºC and 900 ºC, respectively. These results show that the lower ausforming temperature, the higher dislocation density introduced in austenite is. This increase in dislocation density in fresh martensite is explained on the one hand because some of the dislocations are inherited from deformed austenite as it was explained in this work previously. On the other hand, the deformation of austenite refines lath thickness and reduces martensite start temperature as Zhang et al. reported in previous work [47]. In this article Zhang et al. concluded that the lower the ausforming temperature is the higher the lath refinement and the larger the decrease in martensite start temperature are. Bhadeshia and Takahashi reported [48] that the dislocation density (ρ_d) might be estimated by the empirical relationship shown in equation (1). This expression is valid when the martensite start temperature (T) is over the range 297-647 ºC.

$$\text{Log } \rho_d = 9.28480 + \frac{6880}{T} - \frac{1780360}{T^2} \qquad (1)$$

Extracting the data of the martensite start temperature from a previous work [23], where a detailed microstructural characterization was carried out for these thermomechanically treated materials, the estimation of the dislocation density obtained after the different ausforming conditions can be estimated. For the material ausformed at 600 ºC with a martensite start temperature of 338 ºC a dislocation density of $5.97\cdot 10^{15}$ m^{-2} is calculated while for the

material ausformed at 900 ºC with a martensite start temperature of 374 ºC the dislocation density calculated is $4.62 \cdot 10^{15}$ m^{-2}. These results are greater that the values measured by X-Ray diffraction but they are in the same order of magnitude and they demonstrate that the ausforming modifies the martensitic transformation, reducing the martensite start temperature, and in this way allow obtaining higher dislocation density when the ausforming temperature is reduced.

During the final stage (tempering) MX carbonitrides and $M_{23}C_6$ carbides precipitate and the recovery of dislocations take place, improving the toughness. The microstructures of these steels after the thermomechanical treatment consists of tempered martensitic laths with $M_{23}C_6$ carbides on lath, block and prior austenite grain boundaries as shown in Fig. 3. Finer precipitates, MX carbonitrides, are found homogeneously distributed within laths, as can be seen in Fig. 4, pointed out by white arrows. In this figure it is observed that some of MX carbonitrides are located on dislocations, which could demonstrate the potential of dislocations to act as nucleation sites for these precipitates. To measure the spacing and size of MX carbonitrides several TEM micrographs were analyzed and the following equation (2), which correlates the spacing of precipitates λ to the number density N, was used.

$$N = 1/\lambda^3 \quad (2)$$

The size of MX carbonitrides was 5.6 nm and 7.4 nm for the materials ausformed at 600 ºC and 900 ºC, respectively. The size distribution of the precipitates is shown in Fig. 5. The number density of MX carbonitrides was $9.39 \cdot 10^{22}$ m^{-3} for the material ausformed at 600 ºC and $6.4 \cdot 10^{22}$ m^{-3} for the material ausformed at 900 ºC. The reported values of size and number density of MX carbonitrides after conventional processing were 30 nm and 10^{20} m^{-3}, respectively [49]. Therefore, after the ausforming, precipitates size is reduced up to five times and the number density is increased up to two orders of magnitude. In fact, these number densities and precipitates sizes are very similar to those corresponding to oxides in oxide dispersion strengthened (ODS) steels [50, 51].

The high number density of MX carbonitrides obtained after the thermomechanical treatment is stimulated by the large number of nucleation sites introduced during ausforming in the form of dislocations. This is the reason why ausforming triggered finer precipitation and higher number density of MX carbonitrides at 600 ºC compared to 900 ºC.

3.2. Creep behavior by means of Small Punch Creep tests (SPCT).

As an example Fig 6. shows characteristic SPCT curves at 200 N exhibiting the variation of specimen deflection with time for all samples tested. The curve exhibits the three stages of creep similar to those obtained from a uniaxial creep tests. First, after the instantaneous deflection, bending is the main deformation mode in primary stage. This stage is characterized by a decrease in deflection rate. In the secondary and tertiary stage stretching is the prominent deformation mode. Localization of deformation, nucleation and propagation of cracks take place during tertiary stage boosting the deflection rate until the final fracture. In addition, it can be observed from Fig. 7 that a variation in load causes changes in the shape of SPCT curve. When the load increases, the minimum disk deflection rate increases and the time to rupture are reduced significantly.

An important parameter that can be evaluated using SPCT is the minimum disk deflection rate. The variation of disk deflection rate on the applied load is described by a power law relationship, which is similar to expression used in conventional creep known as Norton´s law. The relationship in SPCT is:

$$\delta_d = AF^n \tag{3}$$

Where δ_d is the minimum disk deflection rate, A is a temperature dependent constant, F is the force applied on specimen and n is force exponent.

The Norton Law can be rewritten in the following way:

$$Ln\left(\frac{\delta_d}{\delta_{d200N}}\right) = Ln\left(\frac{A}{\delta_{d200N}}\right) + n \cdot Ln(F) \tag{4}$$

Where δ_{d200N} is the minimum disk deflection rate obtained at the load of 200N for each processing condition. The representation of $Ln\left(\frac{\delta_d}{\delta_{d200N}}\right)$ vs $Ln(F)$ (Fig. 8) allows determining the force exponent “n” (slope) that is related with creep mechanism. The P91 steel, which results are presented in Fig 8, presents the chemical composition shown in table 3 and the heat treatment listed on table 4. The value of R^2, 0.98, suggests that all the samples tested obey the same creep mechanism. Thus, from this result it can be deduced that the thermomechanical treatment does not affect the creep mechanism. The characteristic value of the exponent n for the materials is found to be 5.5. A value of 6 for the stress exponent was referenced by Abe et. al [52] in G91 steels at low stresses. The value of 5.5 implies that creep deformation mechanism is controlled by dislocation motion. It should, however, be noted that the exponent

n is not exactly the same as the one obtained from uniaxial creep tests. In the SPCT, the equivalent stress is not homogeneous within the sample. Moreover, the stress level is increasing with increasing deflection (time). Nevertheless, it is meaningful to compare the load exponent of various SPC tests.

From Fig. 9 it is evident that P91, processed by the conventional heat treatment, exhibits higher minimum disk deflection rate than the samples processed by thermomechanical treatments at the same load, exhibiting the lowest minimum disk deflection rate the material ausformed at the lowest temperature.

These results suggest that MX carbonitrides act as efficient obstacles to dislocations motion during creep, and hence decrease the minimum creep rate. This behavior explains that the material with the highest number density of MX develops the lowest minimum disk deflection rate.

The log plot of variation of creep rupture life with load is presented in Fig. 10. The samples after the thermomechanical treatments exhibit higher creep rupture strength than the P91 steel after conventional heat treatment. There is significant difference between the steels processed by the thermomechanical treatments. A higher creep rupture strength is obtained for the sample processed at the lowest ausforming temperature. The same trend was observed with the minimum disk deflection rate, which indicates that the pinning effect of MX carbonitrides on dislocations during creep allows retarding the onset of acceleration creep increasing considerably the time to rupture.

Nevertheless, the fractographic examination of SPCT samples leads to brittle failure for the samples processed by thermomechanical treatments, i.e. lower reduction in thickness and radial cracks were observed as compared to conventionally treated P91. The fracture mechanism and the microstructural degradation during creep that produce this change in ductility is under investigation and it is going to be reported in a separated paper.

4. Conclusions

The SPCT was applied to evaluate the creep behavior of G91 steel after different heat and thermomechanical treatments. The minimum disk deflection rate was lower and the time to rupture was longer for G91 after thermomechanical treatments as compared to the conventional G91 heat treatment. There is a significant difference in the minimum disk deflection rate as well as in the time to rupture among the G91 samples processed by different thermomechanical treatments. The steel deformed at the lowest ausforming temperature showed the slowest minimum disk deflection rate and the longest time to rupture. The

improvement in creep rupture strength is attributed to the fine and homogeneous distribution of MX carbonitrides. These precipitates, after the thermomechanical treatments exhibited, a number density up to two times higher and an average size up to five times smaller than that after the conventional heat treatment. The highest number density and the smallest average precipitate size were obtained for the materials ausformed at the lowest temperature. This fact is explained according to XRD measurements, which showed that the dislocation density introduced during ausforming was higher at 600 ºC than at 900 ºC. These dislocations act as nucleation sites for precipitates, promoting the formation of finer MX with a higher number density. The force exponent calculated through Norton´s power law had a value close to 6 for all the samples tested, which suggest that the dislocations motion controls the operating creep mechanism. Therefore, it can be concluded that MX carbonitrides act as efficient obstacles for the motion of dislocations during creep. MX pinning of dislocations slow down minimum disk deflection rate and extends the time to rupture.

The number density and average precipitate size of MX carbonitrides after the thermomechanical treatment are similar to the oxide particles in ODS steels. These steels possess high creep strength due to their high number density of oxides distributed in the matrix [53, 54]. Considering MX carbonitrides as a substitute for oxides, 9Cr ferritic/ martensitic steels after the thermomechanical treatment are a potential replacement of ODS steels, which are fabricated by expensive powder metallurgy and mechanical alloying processing routes.

Acknowledgments.

Authors acknowledge financial support to Spanish Ministerio de Economia y Competitividad (MINECO) through in the form of a Coordinate Project (MAT2016-80875-C3-1-R). Authors also would like to acknowledge financial support to Comunidad de Madrid through DIMMAT-CM_S2013/MIT-2775 project. The authors are grateful for the dilatometer tests by Phase Transformation laboratory. J.Vivas acknowledges financial support in the form of a FPI Grant BES-2014-069863. This work contributes to the Joint Programme on Nuclear Materials (JPNM) of the European Energy Research Alliance (EERA).

References.

[1] F. Abe, Bainitic and martensitic creep-resistant steels, Current Opinion in Solid State and Materials Science 8(3–4) (2004) 305-311.

[2] R.L. Klueh, D.S. Gelles, S. Jitsukawa, A. Kimura, G.R. Odette, B. van der Schaaf, M. Victoria, Ferritic/martensitic steels – overview of recent results, Journal of Nuclear Materials 307–311, Part 1(0) (2002) 455-465.
[3] S.J. Zinkle, G.S. Was, Materials challenges in nuclear energy, Acta Materialia 61(3) (2013) 735-758.
[4] R.L. Klueh, A.T. Nelson, Ferritic/martensitic steels for next-generation reactors, Journal of Nuclear Materials 371(1–3) (2007) 37-52.
[5] R.L. Klueh, K. Ehrlich, F. Abe, Ferritic/martensitic steels: promises and problems, Journal of Nuclear Materials 191–194, Part A(0) (1992) 116-124.
[6] F. Masuyama, History of Power Plants and Progress in Heat Resistant Steels, ISIJ International 41(6) (2001) 612-625.
[7] K.H. Mayer, F. Masuyama, 2 - The development of creep-resistant steels, Creep-Resistant Steels, Woodhead Publishing2008, pp. 15-77.
[8] F. Abe, Precipitate design for creep strengthening of 9% Cr tempered martensitic steel for ultra-supercritical power plants, Science and Technology of Advanced Materials 9(1) (2008) 15.
[9] F. Abe, Coarsening behavior of lath and its effect on creep rates in tempered martensitic 9Cr–W steels, Materials Science and Engineering: A 387 (2004) 565-569.
[10] F. Abe, T. Horiuchi, M. Taneike, K. Sawada, Stabilization of martensitic microstructure in advanced 9Cr steel during creep at high temperature, Materials Science and Engineering: A 378(1–2) (2004) 299-303.
[11] O. Prat, J. García, D. Rojas, J.P. Sanhueza, C. Camurri, Study of nucleation, growth and coarsening of precipitates in a novel 9%Cr heat resistant steel: Experimental and modeling, Materials Chemistry and Physics 143(2) (2014) 754-764.
[12] F. Abe, S. Nakazawa, H. Araki, T. Noda, The role of microstructural instability on creep behavior of a martensitic 9Cr-2W steel, Metallurgical Transactions A 23(2) (1992) 469-477.
[13] L. Maddi, D. Barbadikar, M. Sahare, A.R. Ballal, D.R. Peshwe, R.K. Paretkar, K. Laha, M.D. Mathew, Microstructure Evolution During Short Term Creep of 9Cr–0.5Mo–1.8W Steel, Transactions of the Indian Institute of Metals 68(2) (2015) 259-266.
[14] H. Ghassemi-Armaki, R.P. Chen, K. Maruyama, M. Igarashi, Contribution of recovery mechanisms of microstructure during long-term creep of Gr.91 steels, Journal of Nuclear Materials 433(1–3) (2013) 23-29.
[15] R.L. Klueh, N. Hashimoto, P.J. Maziasz, Development of new nano-particle-strengthened martensitic steels, Scripta Materialia 53(3) (2005) 275-280.

[16] S. Hollner, B. Fournier, J. Le Pendu, T. Cozzika, I. Tournié, J.C. Brachet, A. Pineau, High-temperature mechanical properties improvement on modified 9Cr–1Mo martensitic steel through thermomechanical treatments, Journal of Nuclear Materials 405(2) (2010) 101-108.
[17] L. Tan, J.T. Busby, P.J. Maziasz, Y. Yamamoto, Effect of thermomechanical treatment on 9Cr ferritic–martensitic steels, Journal of Nuclear Materials 441(1–3) (2013) 713-717.
[18] S. Li, Z. Eliniyaz, F. Sun, Y. Shen, L. Zhang, A. Shan, Effect of thermo-mechanical treatment on microstructure and mechanical properties of P92 heat resistant steel, Materials Science and Engineering: A 559(0) (2013) 882-888.
[19] L. Tan, Y. Yang, J.T. Busby, Effects of alloying elements and thermomechanical treatment on 9Cr Reduced Activation Ferritic–Martensitic (RAFM) steels, Journal of Nuclear Materials 442(1–3, Supplement 1) (2013) S13-S17.
[20] R.L. Klueh, N. Hashimoto, P.J. Maziasz, New nano-particle-strengthened ferritic/martensitic steels by conventional thermo-mechanical treatment, Journal of Nuclear Materials 367–370, Part A(0) (2007) 48-53.
[21] M. Song, C. Sun, Z. Fan, Y. Chen, R. Zhu, K.Y. Yu, K.T. Hartwig, H. Wang, X. Zhang, A roadmap for tailoring the strength and ductility of ferritic/martensitic T91 steel via thermo-mechanical treatment, Acta Materialia 112 (2016) 361-377.
[22] J. Vivas, C. Celada-Casero, D. San Martín, M. Serrano, E. Urones-Garrote, P. Adeva, M.M. Aranda, C. Capdevila, Nano-precipitation Strengthened G91 by Thermo-mechanical Treatment Optimization, Metallurgical and Materials Transactions A (2016) 1-8.
[23] J. Vivas, C. Capdevila, J. Jimenez, M. Benito-Alfonso, D. San-Martin, Effect of Ausforming Temperature on the Microstructure of G91 Steel, Metals 7(7) (2017) 236.
[24] E. Altstadt, M. Serrano, M. Houska, A. García-Junceda, Effect of anisotropic microstructure of a 12Cr-ODS steel on the fracture behaviour in the small punch test, Materials Science and Engineering: A 654 (2016) 309-316.
[25] X. Jia, Y. Dai, Small punch tests on martensitic/ferritic steels F82H, T91 and Optimax-A irradiated in SINQ Target-3, Journal of Nuclear Materials 323(2–3) (2003) 360-367.
[26] E. Altstadt, H.E. Ge, V. Kuksenko, M. Serrano, M. Houska, M. Lasan, M. Bruchhausen, J.M. Lapetite, Y. Dai, Critical evaluation of the small punch test as a screening procedure for mechanical properties, Journal of Nuclear Materials.
[27] E. Fleury, J.S. Ha, Small punch tests to estimate the mechanical properties of steels for steam power plant: I. Mechanical strength, International Journal of Pressure Vessels and Piping 75(9) (1998) 699-706.

[28] S.P. Singh, S. Bhattacharya, D.K. Sehgal, Evaluation of high temperature mechanical strength of Cr–Mo grade steel through small punch test technique, Engineering Failure Analysis 39 (2014) 207-220.
[29] D. Finarelli, M. Roedig, F. Carsughi, Small punch tests on austenitic and martensitic steels irradiated in a spallation environment with 530 MeV protons, Journal of Nuclear Materials 328(2–3) (2004) 146-150.
[30] C. Rodríguez, M. Fernández, J.G. Cabezas, T.E. García, F.J. Belzunce, The use of the small punch test to solve practical engineering problems, Theoretical and Applied Fracture Mechanics 86, Part A (2016) 109-116.
[31] D. Andrés, R. Lacalle, J.A. Álvarez, Creep property evaluation of light alloys by means of the small punch test: Creep master curves, Materials & Design.
[32] F. Dobeš, K. Milička, Application of creep small punch testing in assessment of creep lifetime, Materials Science and Engineering: A 510–511 (2009) 440-443.
[33] S.-i. Komazaki, T. Kato, Y. Kohno, H. Tanigawa, Creep property measurements of welded joint of reduced-activation ferritic steel by the small-punch creep test, Materials Science and Engineering: A 510–511 (2009) 229-233.
[34] B. Gülçimen, A. Durmuş, S. Ülkü, R.C. Hurst, K. Turba, P. Hähner, Mechanical characterisation of a P91 weldment by means of small punch fracture testing, International Journal of Pressure Vessels and Piping 105–106 (2013) 28-35.
[35] D. Blagoeva, Y.Z. Li, R.C. Hurst, Qualification of P91 welds through Small Punch creep testing, Journal of Nuclear Materials 409(2) (2011) 124-130.
[36] L. Zhao, H. Jing, L. Xu, Y. Han, J. Xiu, Y. Qiao, Evaluating of creep property of distinct zones in P92 steel welded joint by small punch creep test, Materials & Design 47 (2013) 677-686.
[37] Naveena, S.-i. Komazaki, Evaluation of creep rupture strength of high nitrogen ferritic heat-resistant steels using small punch creep testing technique, Materials Science and Engineering: A 676 (2016) 100-108.
[38] B.E. Warren, B.L. Averbach, The Effect of Cold- Work Distortion on X- Ray Patterns, Journal of Applied Physics 21(6) (1950) 595-599.
[39] B.E. Warren, B.L. Averbach, The Separation of Cold- Work Distortion and Particle Size Broadening in X- Ray Patterns, Journal of Applied Physics 23(4) (1952) 497-497.
[40] G.K. Williamson, R.E. Smallman, III. Dislocation densities in some annealed and cold-worked metals from measurements on the X-ray debye-scherrer spectrum, The Philosophical Magazine: A Journal of Theoretical Experimental and Applied Physics 1(1) (1956) 34-46.

[41] S. Takebayashi, T. Kunieda, N. Yoshinaga, K. Ushioda, S. Ogata, Comparison of the Dislocation Density in Martensitic Steels Evaluated by Some X-ray Diffraction Methods, ISIJ International 50(6) (2010) 875-882.
[42] S. Li, Z. Eliniyaz, L. Zhang, F. Sun, Y. Shen, A. Shan, Microstructural evolution of delta ferrite in SAVE12 steel under heat treatment and short-term creep, Materials Characterization 73 (2012) 144-152.
[43] V. Knezevic, G. Sauthoff, J. Vilk, G. Inden, A. Schneider, R. Agamennone, W. Blum, Y. Wang, A. Scholz, C. Berger, J. Ehlers, L. Singheiser, Martensitic/Ferritic Super Heat-resistant 650°C Steels - Design and Testing of Model Alloys, ISIJ International 42(12) (2002) 1505-1514.
[44] G. Miyamoto, N. Iwata, N. Takayama, T. Furuhara, Quantitative analysis of variant selection in ausformed lath martensite, Acta Materialia 60(3) (2012) 1139-1148.
[45] K. Wakasa, C.M. Wayman, The morphology and crystallography of ferrous lath martensite. Studies of Fe-20%Ni-5%Mn—I. Optical microscopy, Acta Metallurgica 29(6) (1981) 973-990.
[46] J. Takahashi, K. Kawakami, J.-i. Hamada, K. Kimura, Direct observation of niobium segregation to dislocations in steel, Acta Materialia 107(Supplement C) (2016) 415-422.
[47] M. Zhang, Y.H. Wang, C.L. Zheng, F.C. Zhang, T.S. Wang, Austenite deformation behavior and the effect of ausforming process on martensite starting temperature and ausformed martensite microstructure in medium-carbon Si–Al-rich alloy steel, Materials Science and Engineering: A 596 (2014) 9-14.
[48] H.K.D.H. Bhadeshia, Bainite in Steels: Theory and Practice, Maney Publishing2015.
[49] L. Tan, L.L. Snead, Y. Katoh, Development of new generation reduced activation ferritic-martensitic steels for advanced fusion reactors, Journal of Nuclear Materials 478 (2016) 42-49.
[50] L. Toualbi, C. Cayron, P. Olier, J. Malaplate, M. Praud, M.H. Mathon, D. Bossu, E. Rouesne, A. Montani, R. Logé, Y. de Carlan, Assessment of a new fabrication route for Fe–9Cr–1W ODS cladding tubes, Journal of Nuclear Materials 428(1) (2012) 47-53.
[51] C. Heintze, F. Bergner, A. Ulbricht, M. Hernández-Mayoral, U. Keiderling, R. Lindau, T. Weissgärber, Microstructure of oxide dispersion strengthened Eurofer and iron–chromium alloys investigated by means of small-angle neutron scattering and transmission electron microscopy, Journal of Nuclear Materials 416(1) (2011) 35-39.
[52] F. ABE, Creep Behavior, Deformation Mechanisms, and Creep Life of Mod.9Cr-1Mo Steel, Metallurgical and Materials Transactions A 46(12) (2015) 5610-5625.

[53] C. Zakine, C. Prioul, D. François, Creep behaviour of ODS steels, Materials Science and Engineering: A 219(1) (1996) 102-108.
[54] J. Malaplate, F. Mompiou, J.L. Béchade, T. Van Den Berghe, M. Ratti, Creep behavior of ODS materials: A study of dislocations/precipitates interactions, Journal of Nuclear Materials 417(1) (2011) 205-208.

Figures

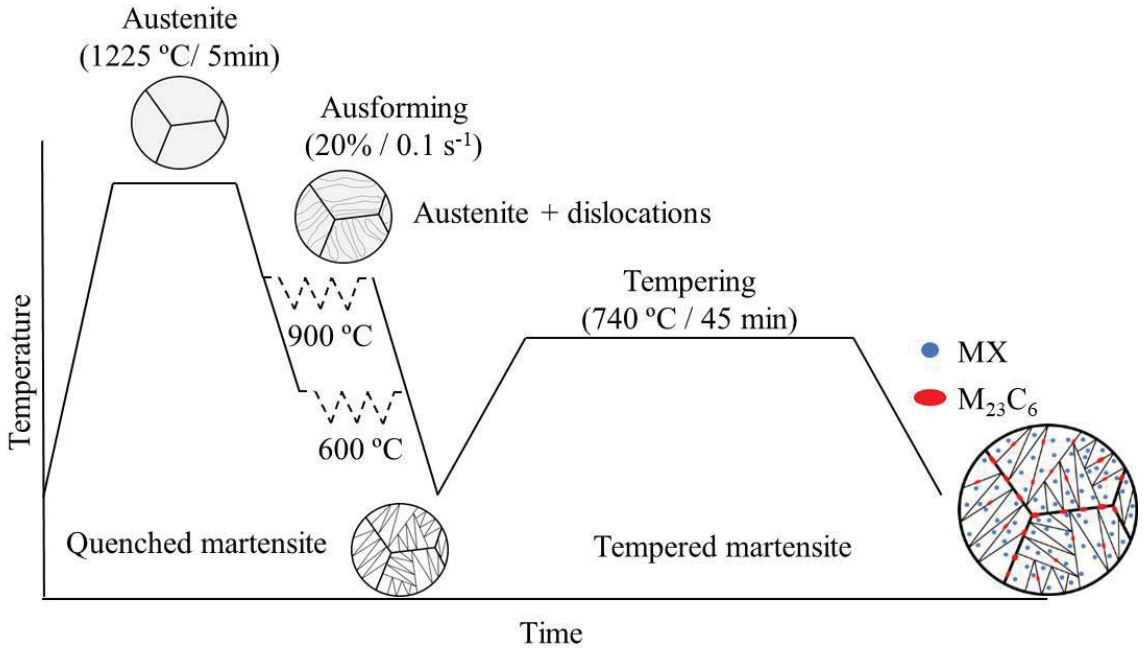

Figure 1. Scheme of thermomechanical treatments (TMT).

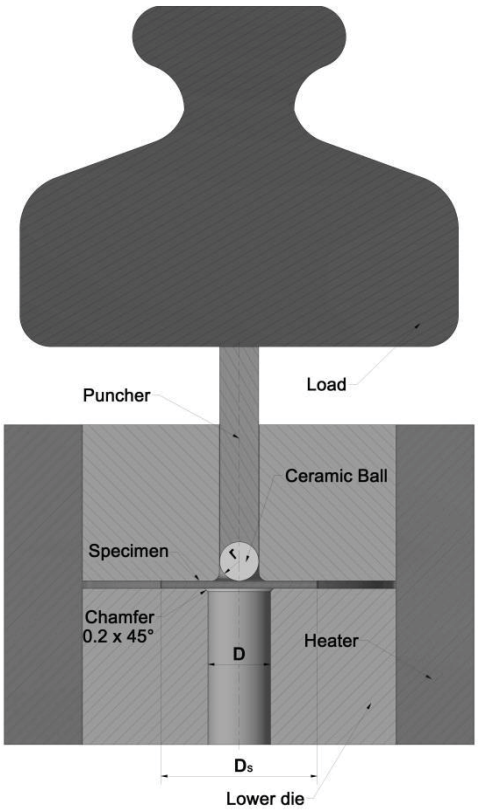

Figure 2. Scheme of the SPC set-up.

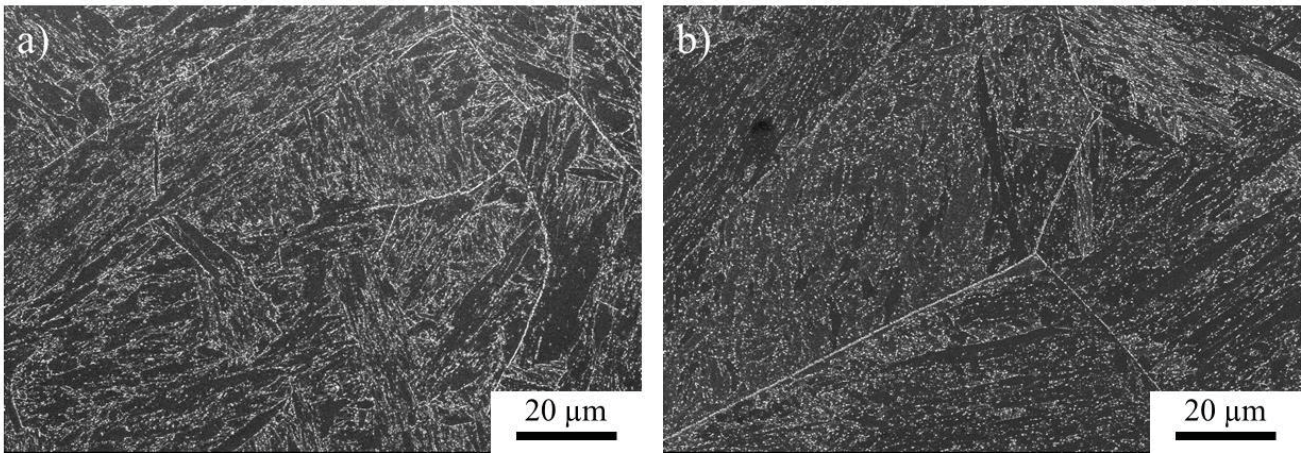

Figure 3. Tempered martensitic microstructure showing $M_{23}C_6$ carbides as white dots after thermomechanical treatment a) ausformed at 900 ºC and b) ausformed at 600ºC.

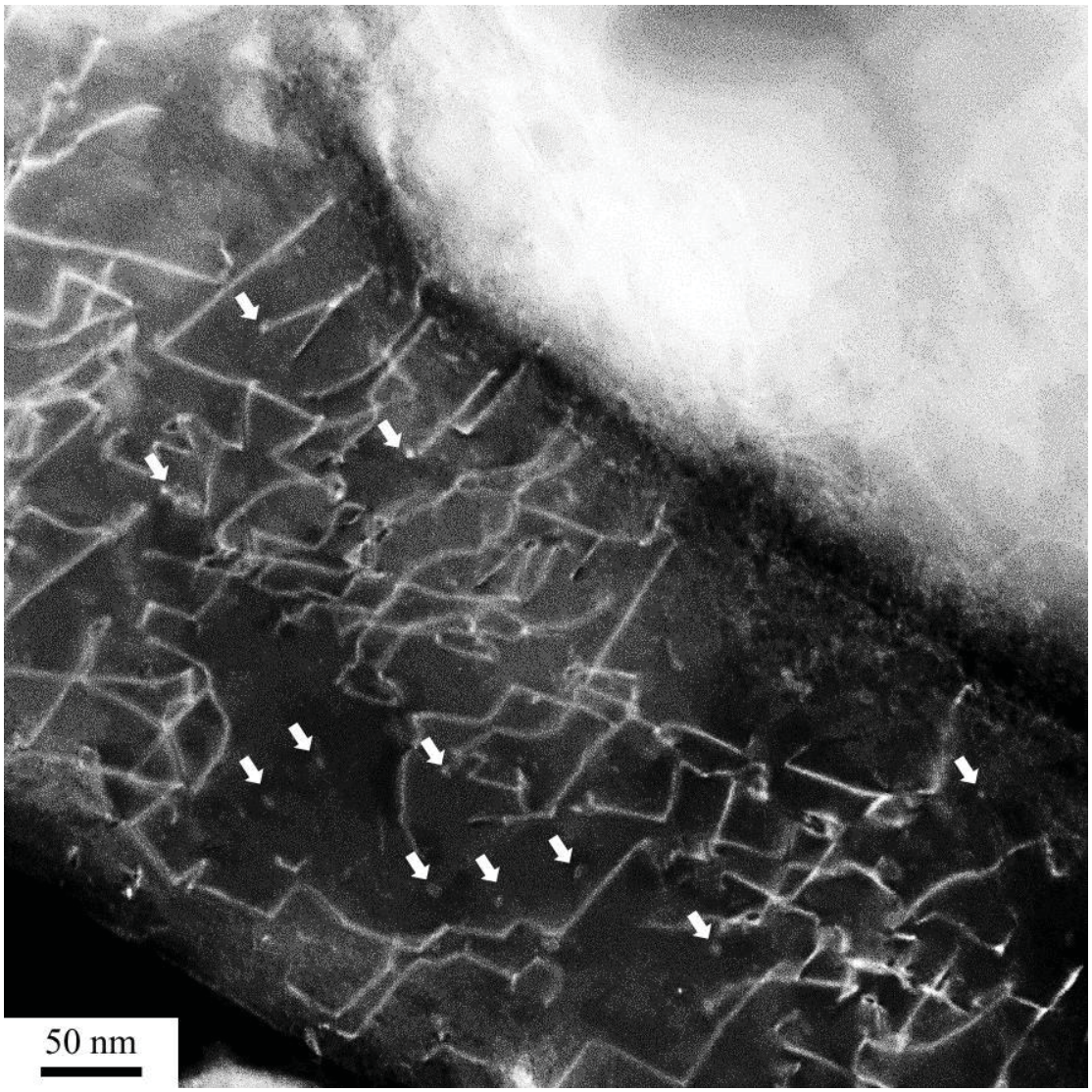

Figure 4. MX carbonitrides within laths after thermomechanical treatment ausformed at 900 ºC.

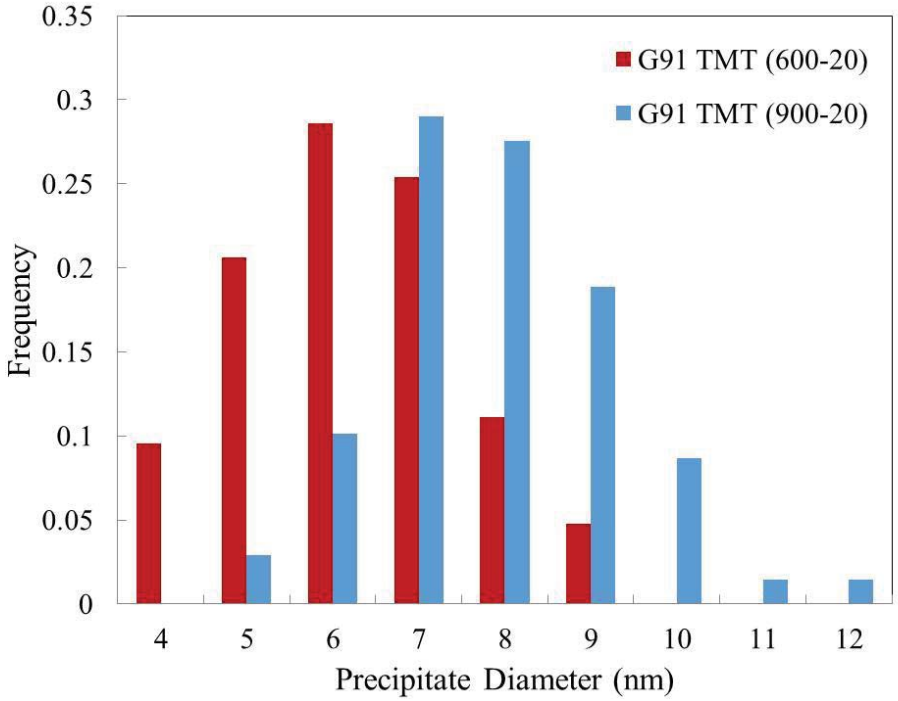

Figure 5. MX precipitates size distribution after thermomechanical treatments.

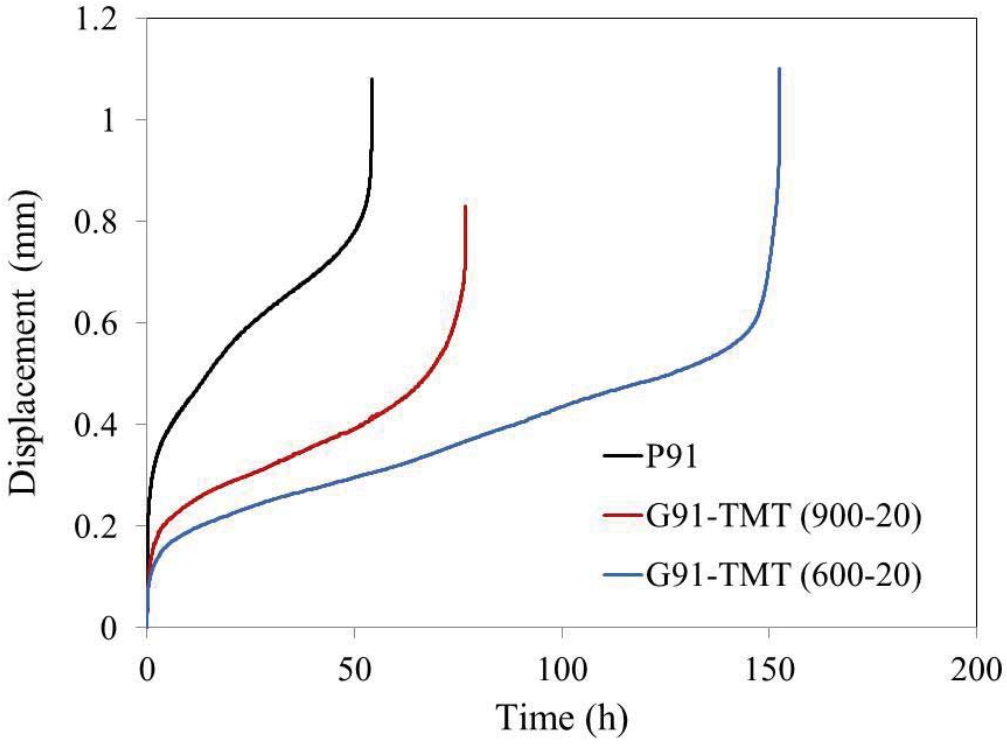

Figure 6. Examples of SPCT curves for all material tested at 700 ºC with a load of 200 N.

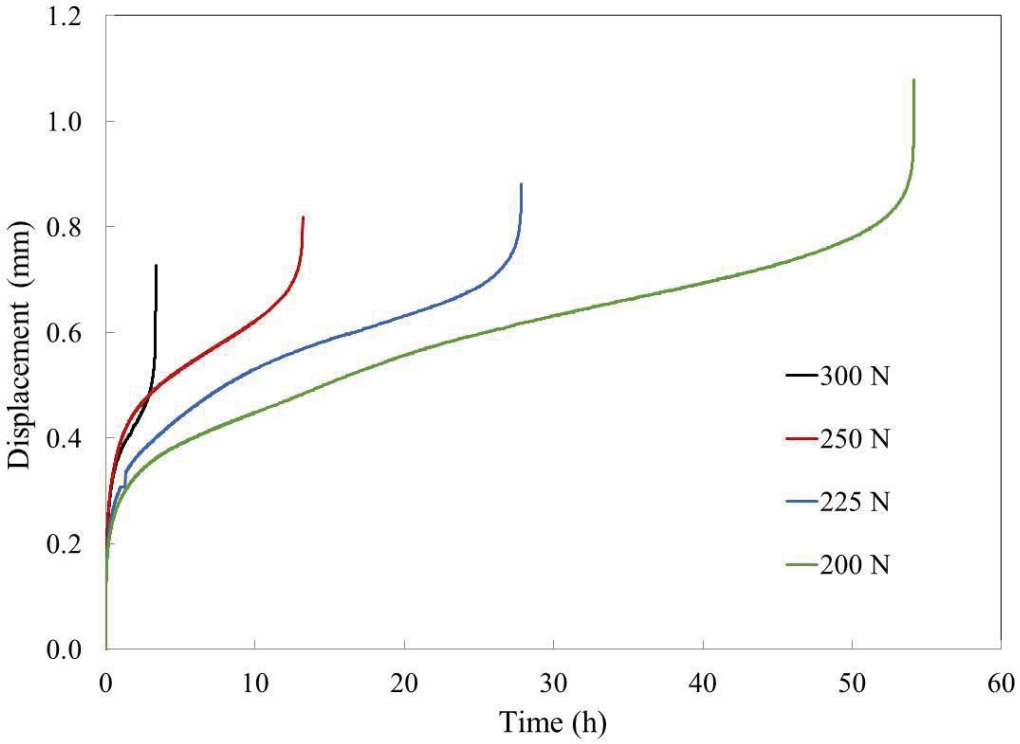

Figure 7. SPCT curves for P91 at 700 ºC and different loads.

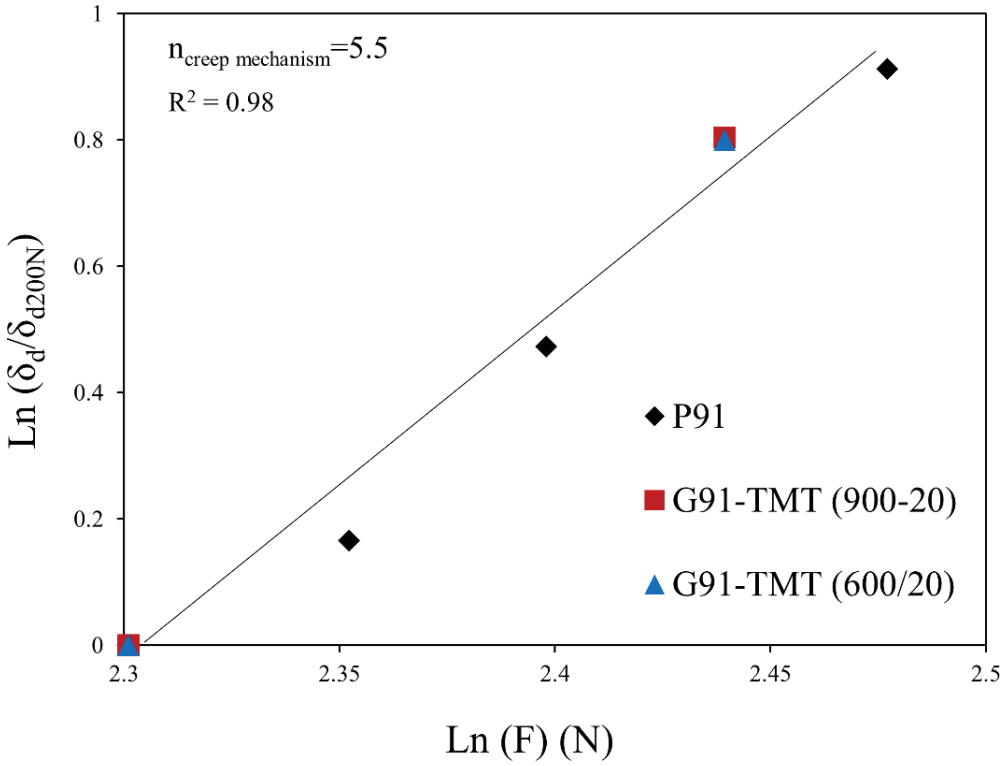

Figure 8. Logarith of normalized minimum disk deflection rate vs logarith of the load.

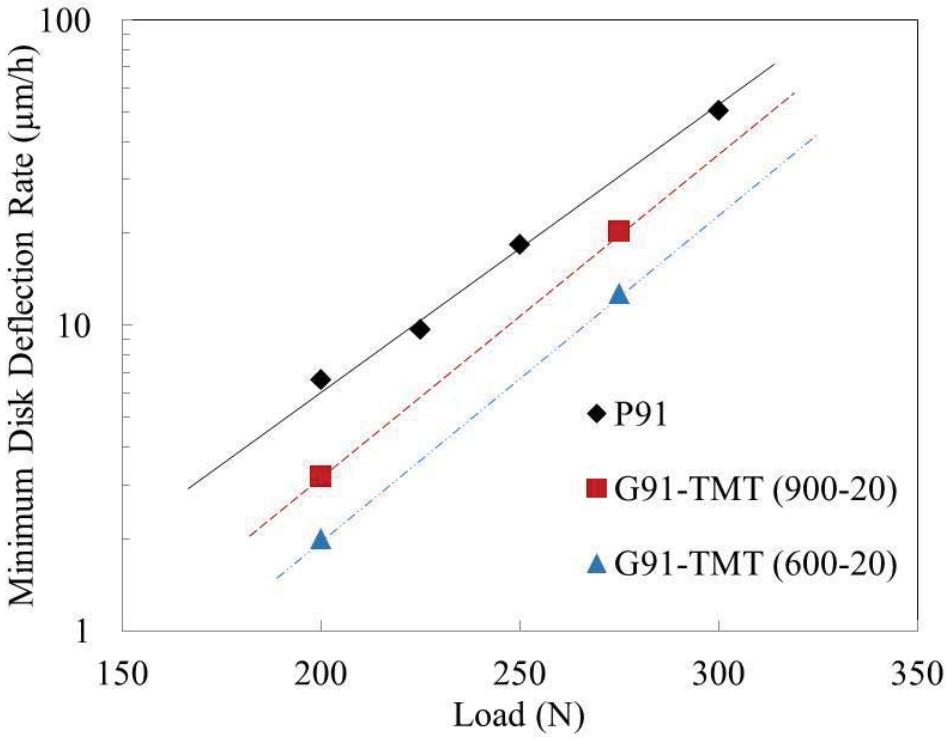

Figure 9. Norton´s law for all materials tested.

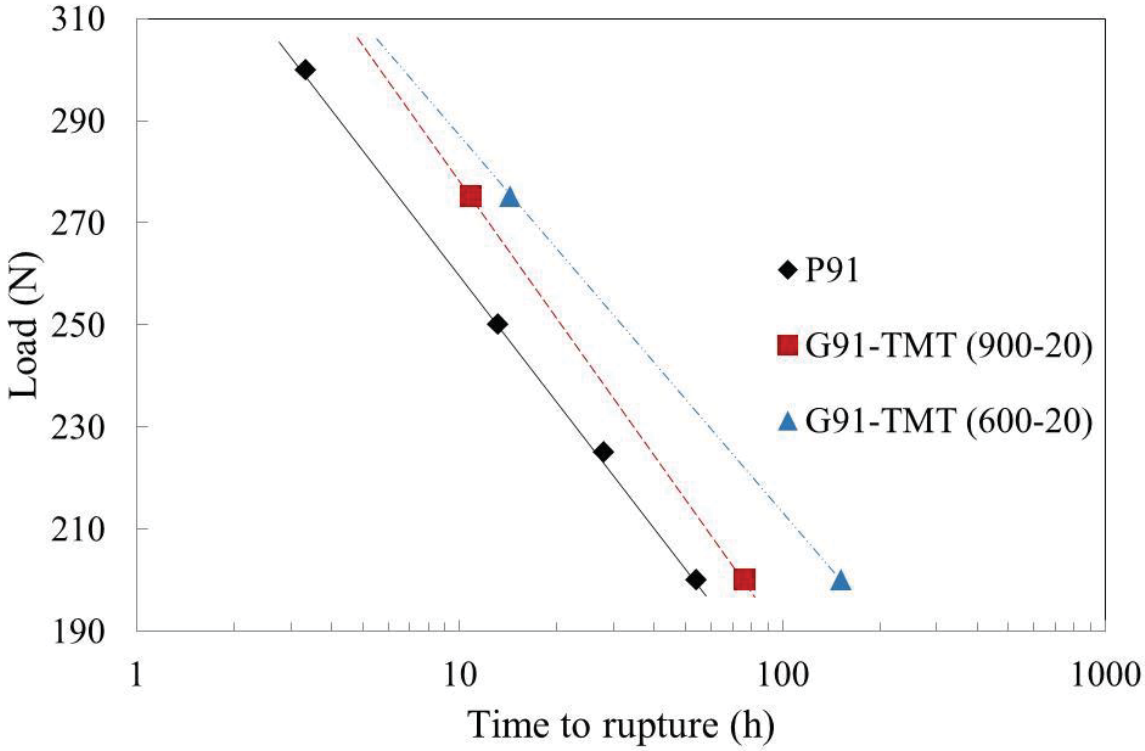

Figure 10. Load vs Time to rupture curves for all materials tested.

Tables

Table 1. Chemical composition of the commercial G91 ferritic-martensitic steel

Elements	C	Si	Mn	Cr	Mo	V	Nb	Fe
Wt. %.	0.09	0. 32	0.60	8.76	0.86	0.18	0.07	balance

Table 2. Small punch creep tests parameters.

Punch diameter d = 2r (mm)	Receiving hole diameter D (mm)	Lower die hole chamfer
2.5	4.0	0.2 mm x 45°

Table 3. Chemical composition of P91 steel

Elements	C	Si	Mn	Cr	Mo	V	Nb	Fe
Wt. %.	0.12	0.46	0.51	9.50	0.91	0.23	0.09	balance

Table 4. Heat treatments of P91

Heat	Product form	Heat treatment
P91	hot rolled pipe ∅360 x 50 mm	normalization 1040 / 30 min tempering 730 / 60 min

Figure(s)
Click here to download high resolution image

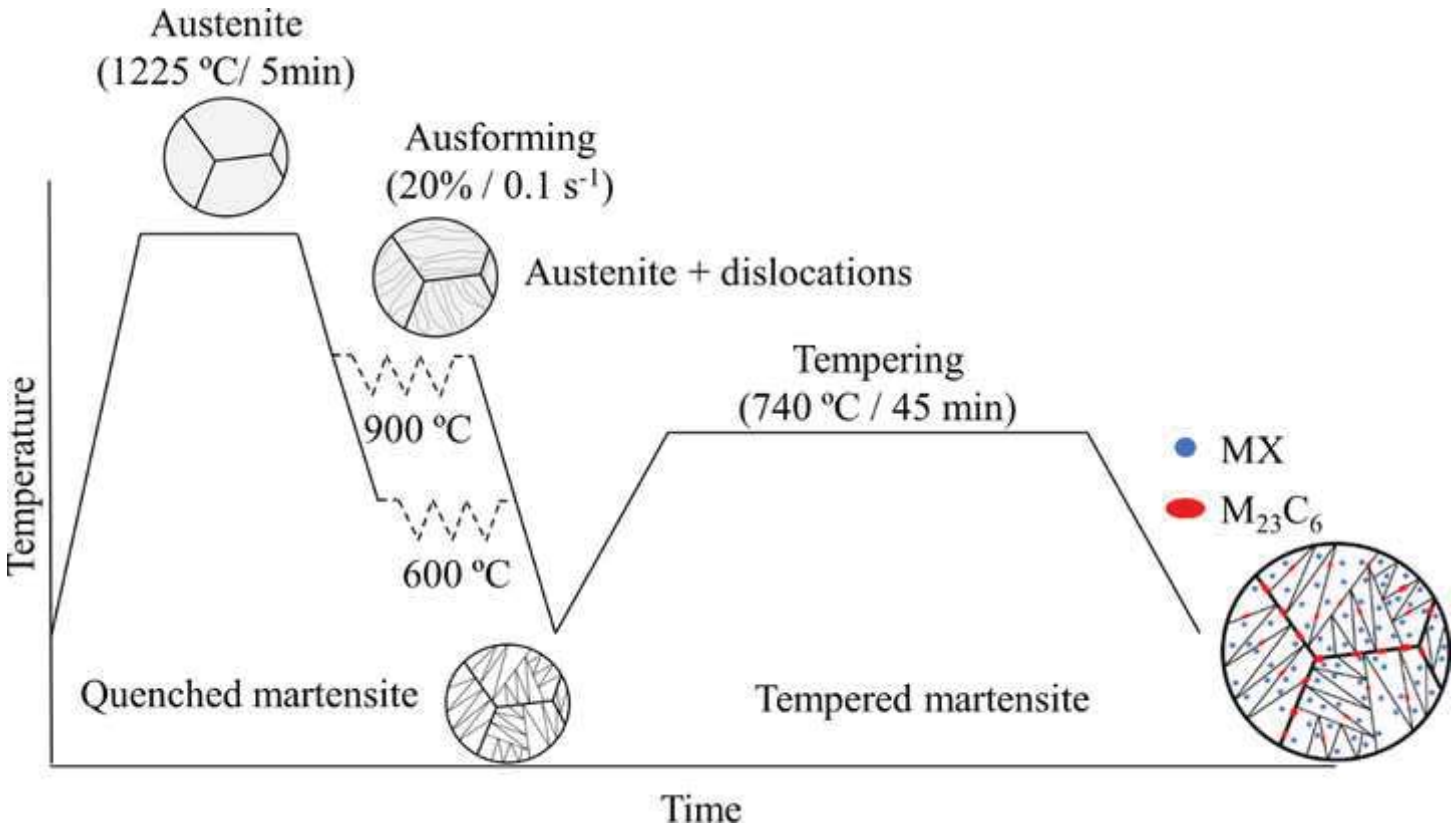

Figure(s)
Click here to download high resolution image

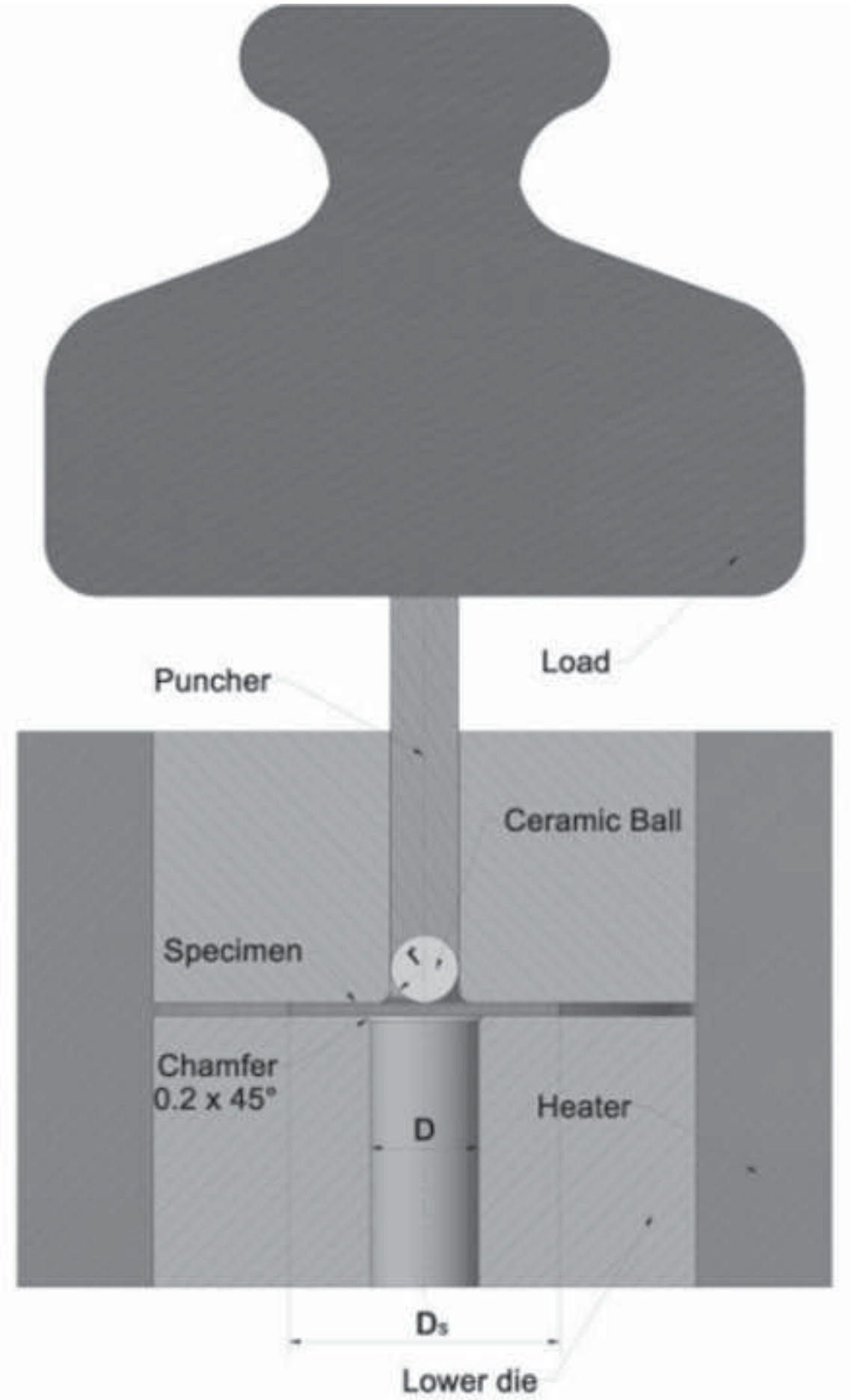

Figure(s)
Click here to download high resolution image

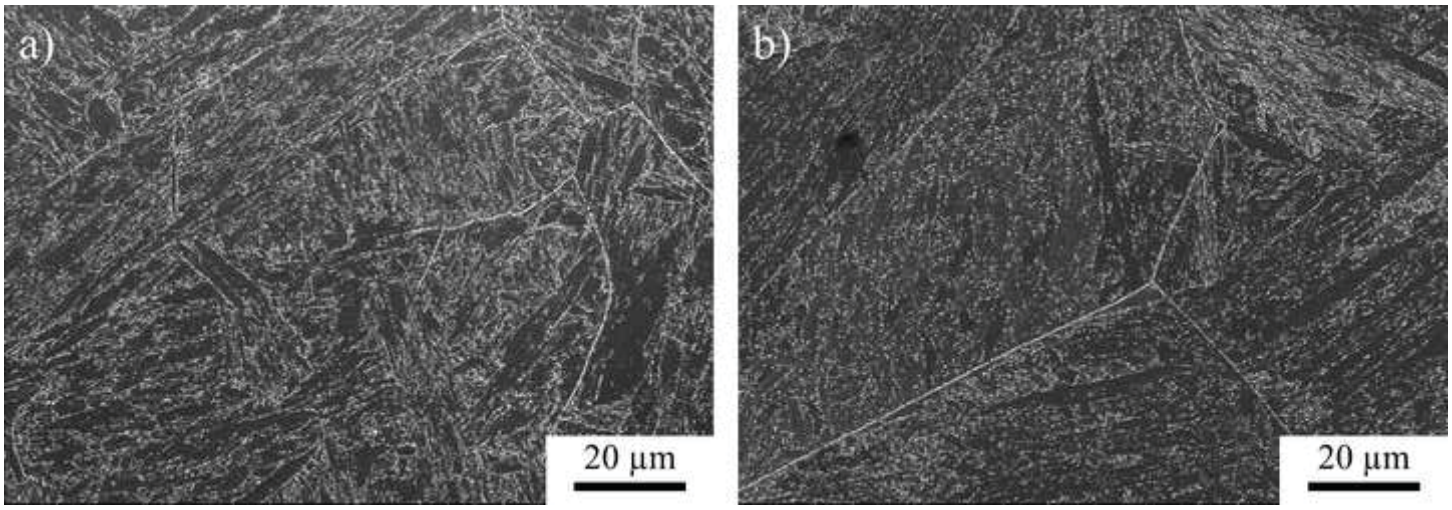

Figure(s)
Click here to download high resolution image

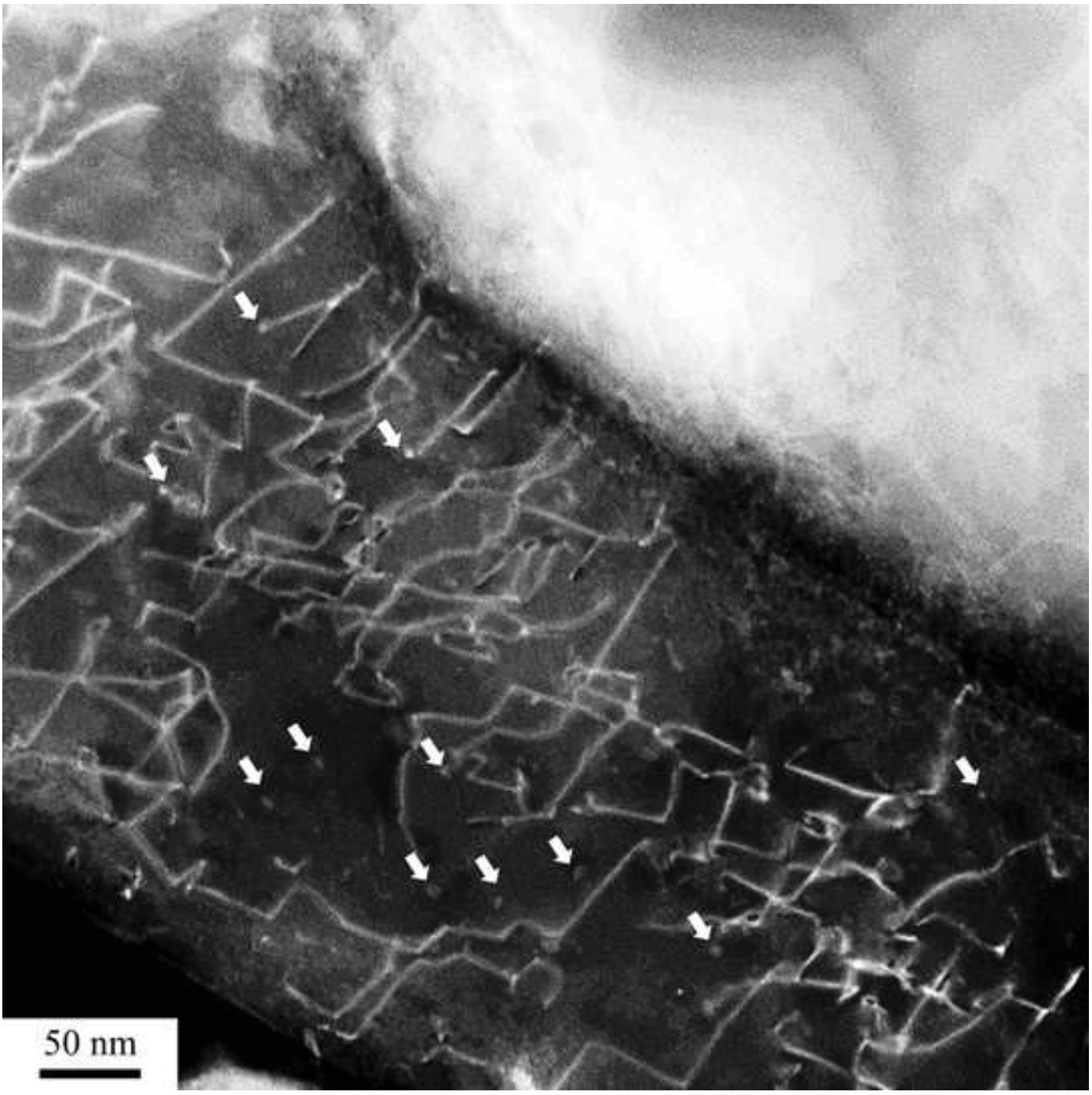

Figure(s)
Click here to download high resolution image

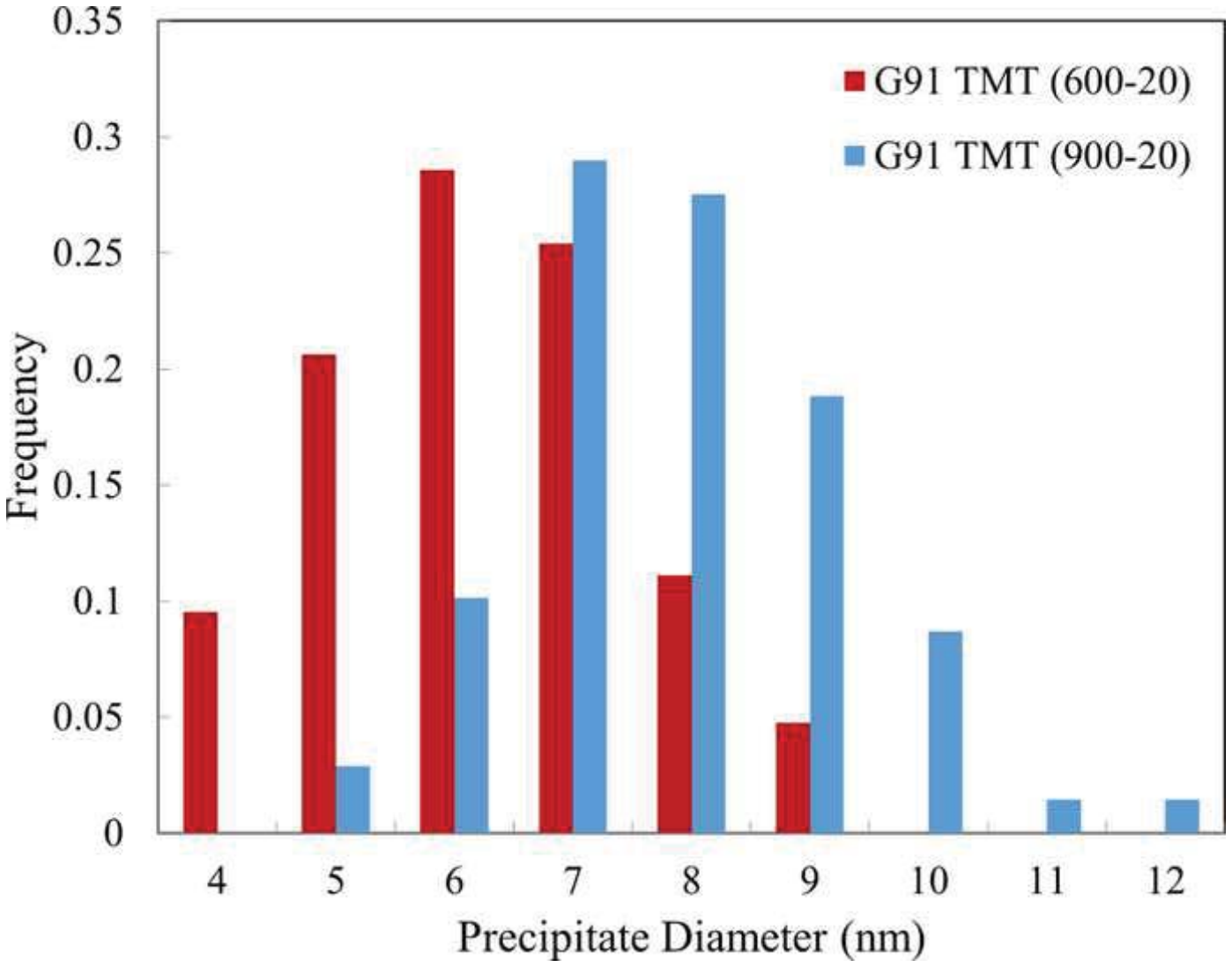

Figure(s)
Click here to download high resolution image

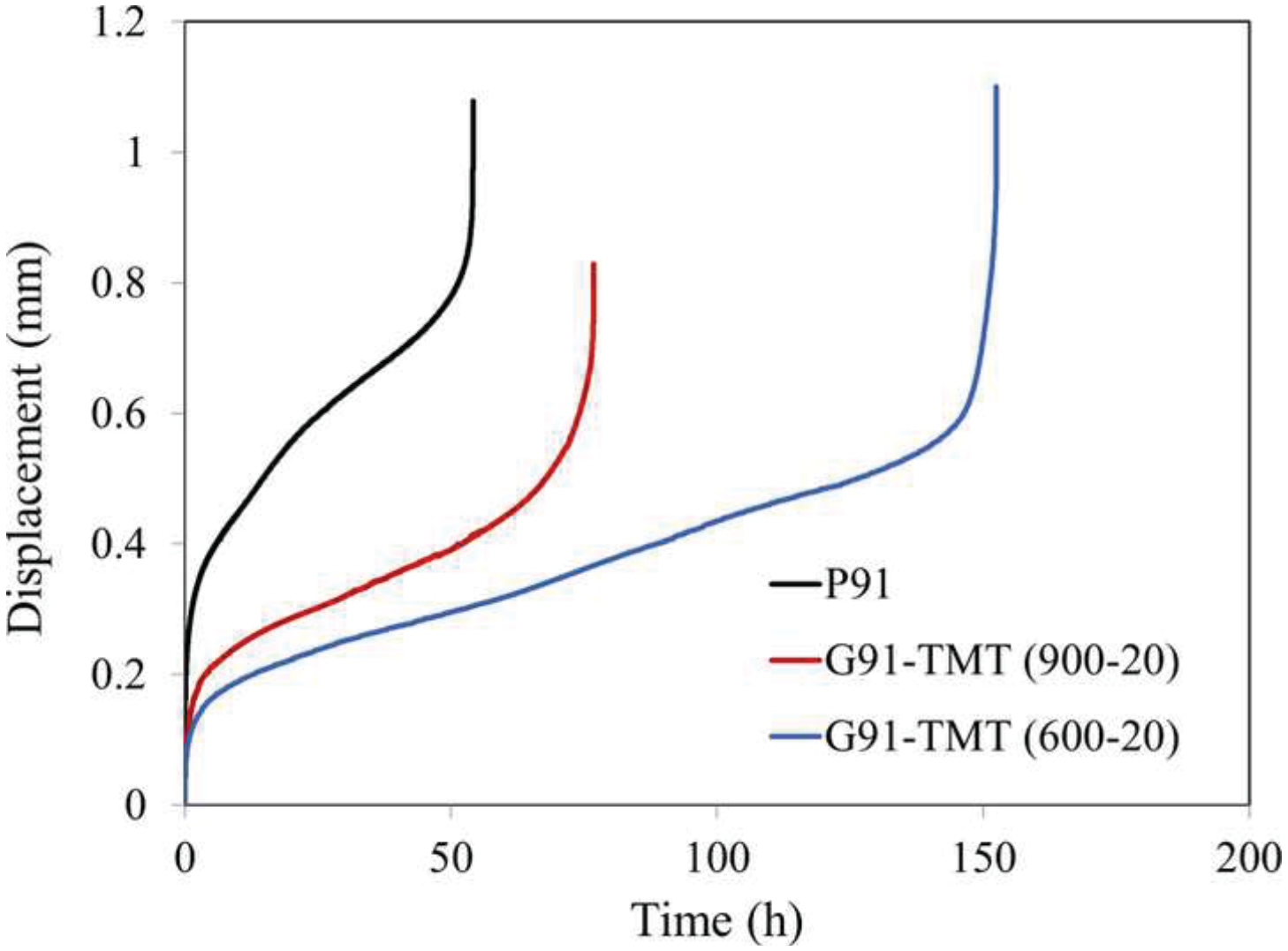

Figure(s)
Click here to download high resolution image

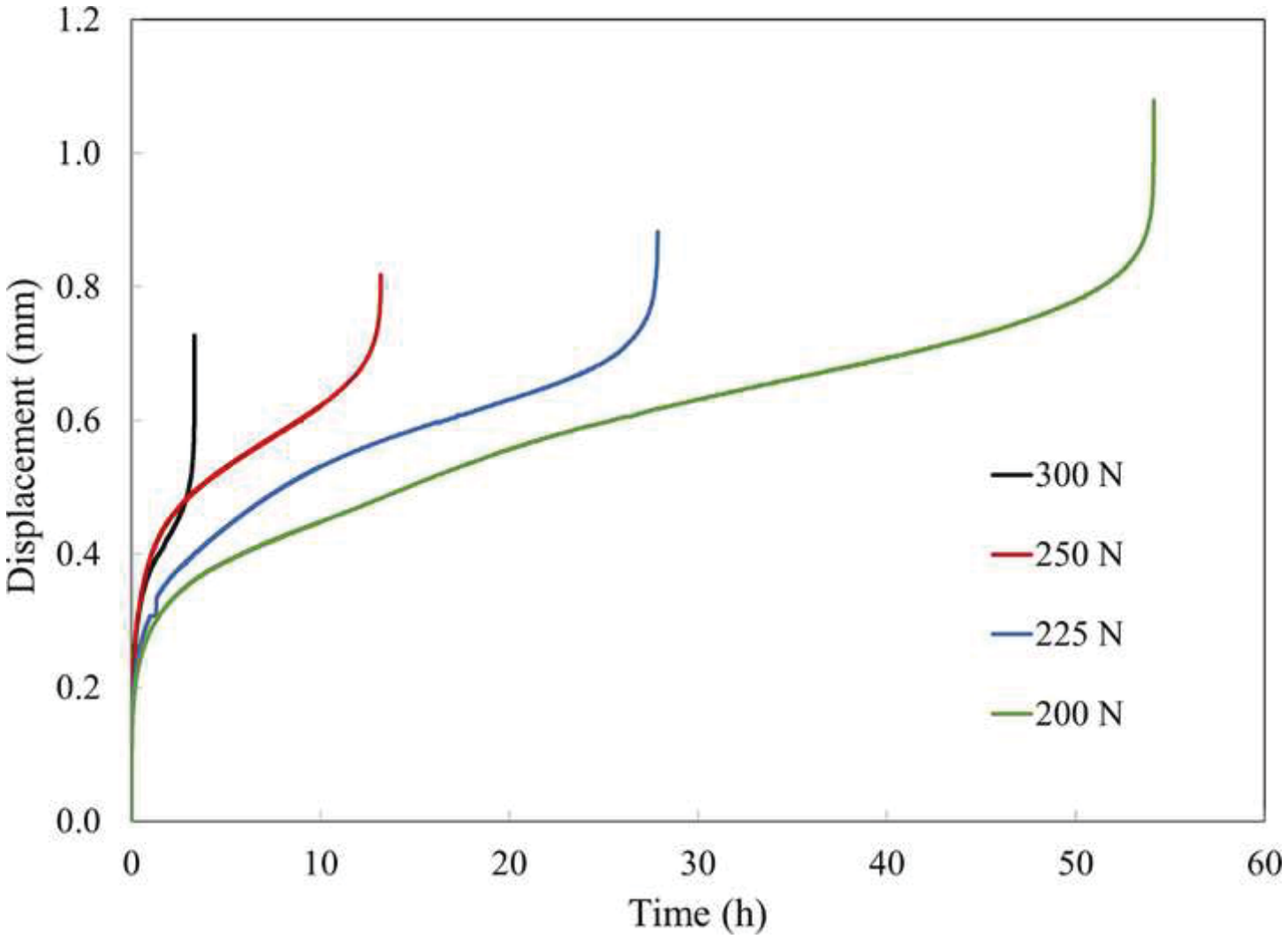

Figure(s)
Click here to download high resolution image

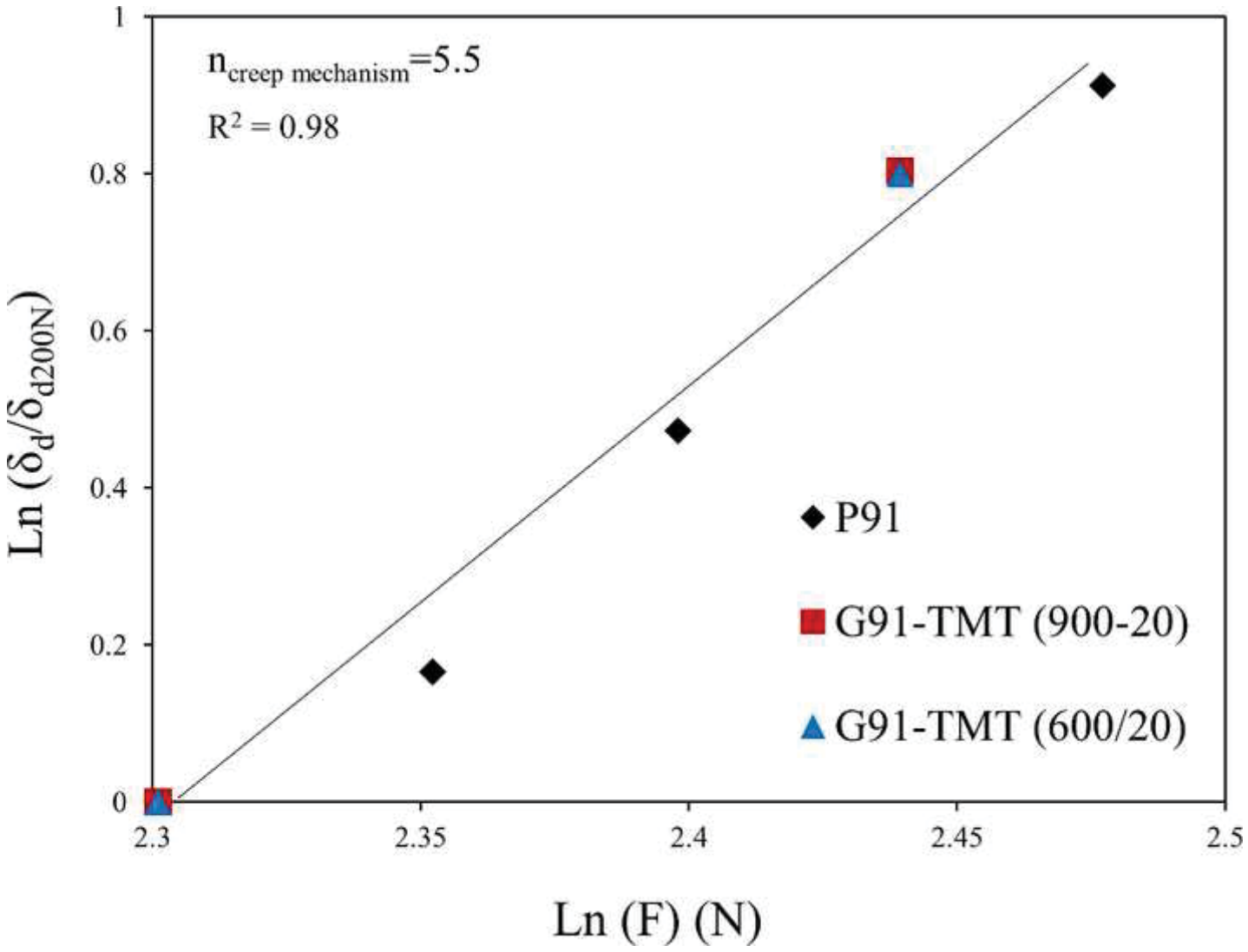

Figure(s)
Click here to download high resolution image

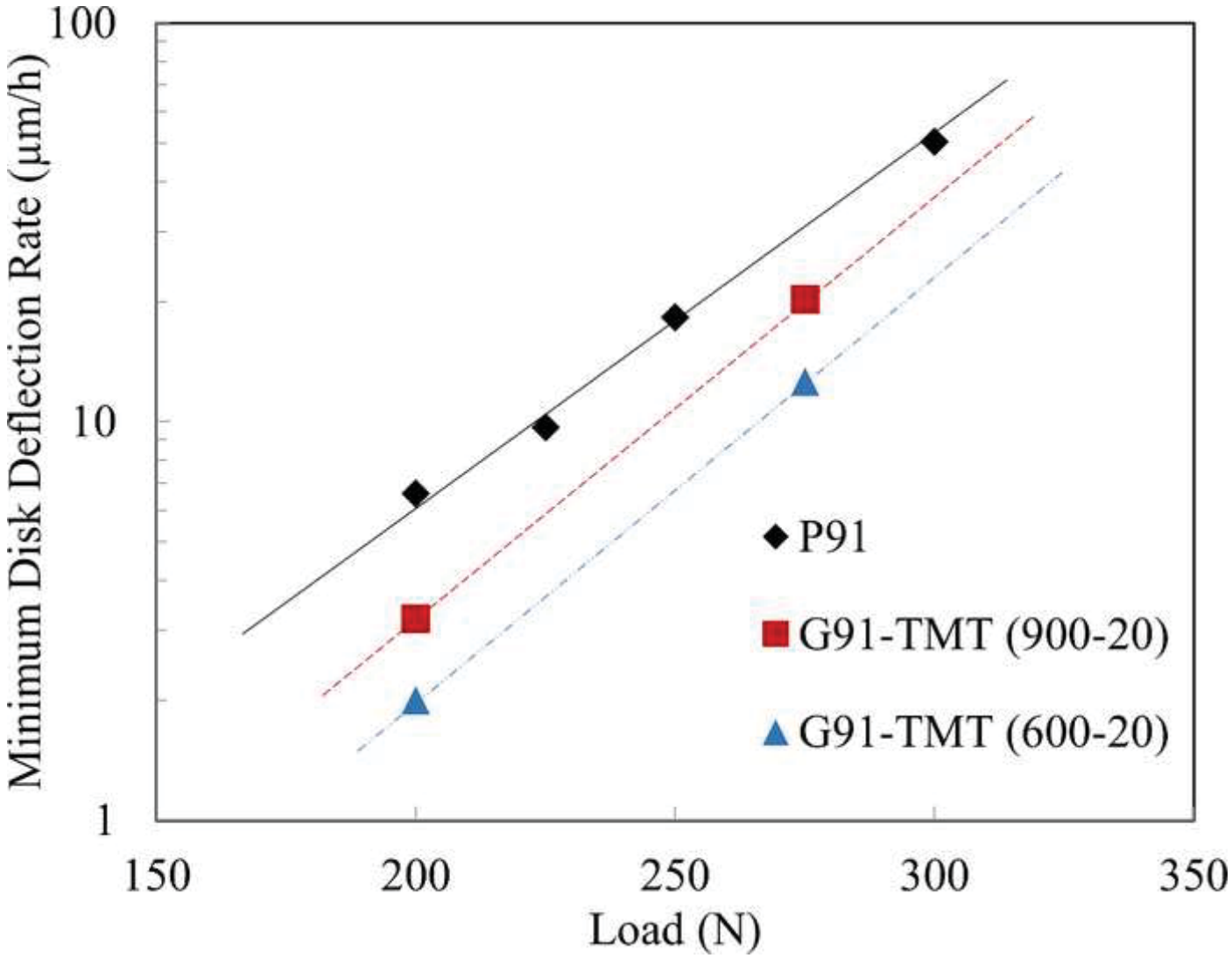

Figure(s)
Click here to download high resolution image

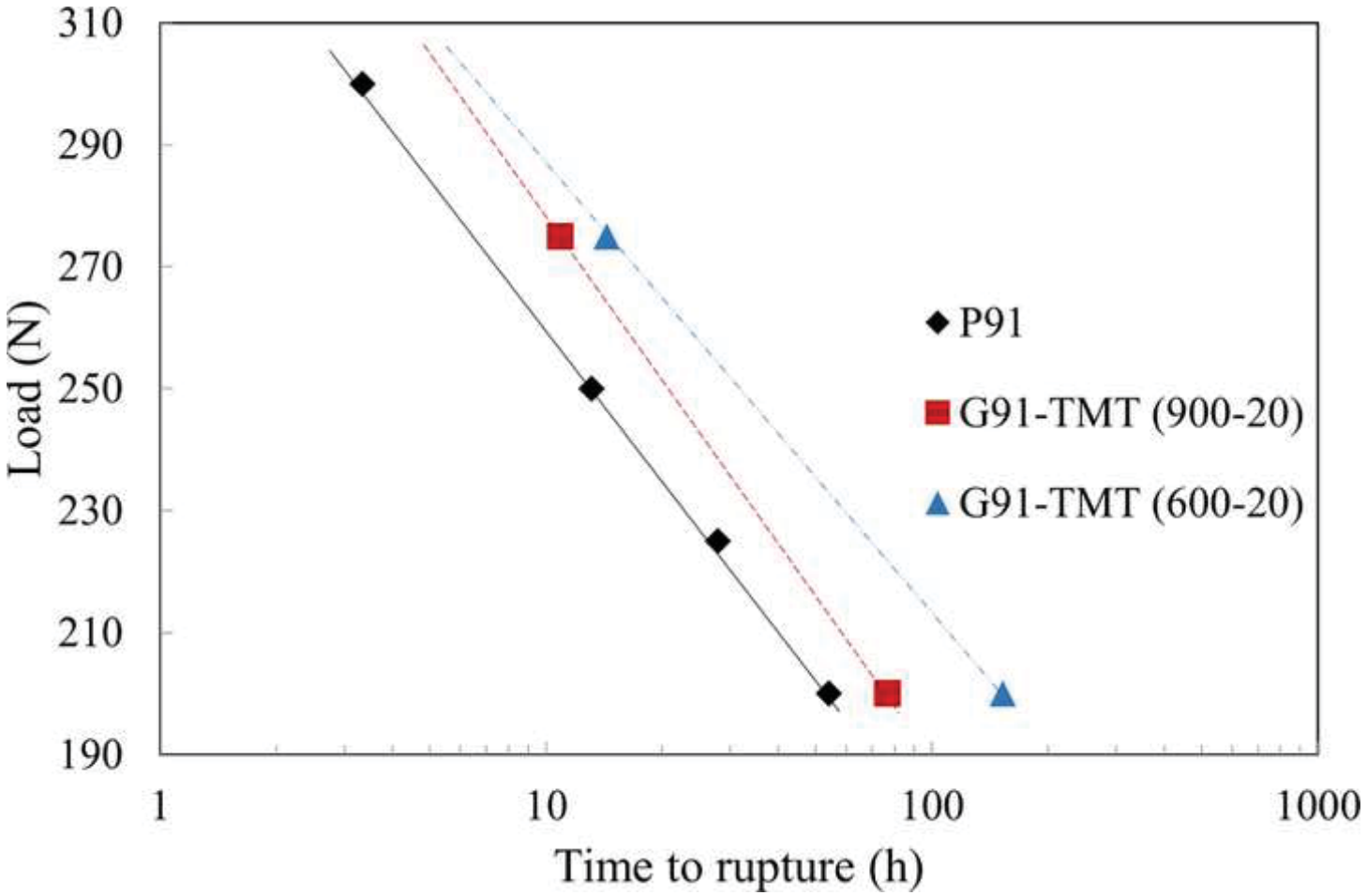

Tables

Table 1. Chemical composition of the commercial G91 ferritic-martensitic steel

Elements	C	Si	Mn	Cr	Mo	V	Nb	Fe
Wt. %.	0.09	0. 32	0.60	8.76	0.86	0.18	0.07	balance

Table 2. Small punch creep tests parameters.

Punch diameter d = 2r (mm)	Receiving hole diameter D (mm)	Lower die hole chamfer
2.5	4.0	0.2 mm x 45°

Table 3. Chemical composition of P91 steel

Elements	C	Si	Mn	Cr	Mo	V	Nb	Fe
Wt. %.	0.12	0.46	0.51	9.50	0.91	0.23	0.09	balance

Table 4. Heat treatments of P91

Heat	Product form	Heat treatment
P91	hot rolled pipe ∅360 x 50 mm	normalization 1040 / 30 min tempering 730 / 60 min